GEM NEWS INTERNATIONAL

Contributing Editors
Gagan Choudhary, *IIGJ-Research & Laboratories Centre, Jaipur, India* (gagan.choudhary@iigjrlc.org)
Christopher M. Breeding, *GIA, Carlsbad* (christopher.breeding@gia.edu)
Guanghai Shi, *School of Gemmology, China University of Geosciences, Beijing* (shigh@cugb.edu.cn)

COLORED STONES AND ORGANIC MATERIALS

New emerald production from the Curlew mine, Western Australia. Australian emeralds have been known for over a century but have always maintained a low profile. Small volumes, low clarity, and desaturated color were among the reasons for their lack of recognition in the global market.

One of Australia's emerald deposits is the Curlew mine in the Shire of East Pilbara in Western Australia. This area has been worked officially since the mid-1970s, but anecdotal evidence suggests that emeralds were known at least 50 years prior to that. During this initial period of mining, the focus was on specimen collecting. Any gem-quality material was sold to Indian-based emerald manufacturers and disappeared into the vast pool of emeralds with undetermined origin.

Figure 1. Emeralds in matrix and various cut stones from the Curlew mine in Western Australia. All stones were mined in 2023. The cut stones are untreated and range from 0.45 to 7.92 ct (triangular shape). Photo by Lhapsin Nillapat; courtesy of Matthew Allen (The Gemstone Trading Company).

From the 1980s to 2011, the mine was largely abandoned, although a few (unsuccessful) attempts were made to revitalize the deposit. In 2011, a prospecting license was passed between different groups with little success in emerald production. In recent years, the mining license was taken over by a small-scale mining group. They successfully produced gem-quality material from the existing pit during the 2023 mining season. Production was limited to a few kilograms of gem-quality material, but the owners intend to scale up the production in 2024.

GIA's Bangkok laboratory was able to study a suite of 69 emeralds from this recent production (figure 1) that was on loan from the miner. The rough emerald crystals showed a well-formed hexagonal outline, often coated with dark mica crystals. Other minerals associated with the emerald were identified as feldspar and quartz. One of the matrix specimens also contained significant volumes of purple fluorite (confirmed by Raman spectroscopy).

The combination of these matrix minerals, especially mica, suggests that these stones formed in the contact zone of a pegmatite intrusion into an (ultra-)mafic rock. Images from the emerald mineralization in the field confirmed this (figure 2). This type of geological environment, found at many other emerald deposits around the world, is responsible for the majority of emeralds in the marketplace, including Kafubu (Zambia), the Ural Mountains (Russia), Shakiso (Ethiopia), and Itabira (Brazil).

Editors' note: Interested contributors should send information and illustrations to Stuart Overlin at soverlin@gia.edu.

Gems & Gemology, Vol. 60, No. 2, pp. 252–270.

Figure 2. An emerald pocket at the reaction zone between the pale pegmatite intrusion (bottom right) and ultramafic greenish rock (top left). The emeralds are encrusted in dark mica crystals. Photo by Matthew Allen; field of view approximately 50 cm.

The refractive index of the stones was 1.580–1.586 ± 0.001, with a birefringence of 0.007. This is in the higher range for emerald and corresponds with other emeralds that form in a similar geological environment.

Chemical analysis using laser ablation–inductively coupled plasma–mass spectrometry (LA-ICP-MS; see table 1) and spectroscopic analysis confirmed that these emeralds were rich in iron. Ultraviolet/visible/near-infrared spectroscopy revealed chromium-related absorption features as well as a strong band around 810 nm, which is attributed to the higher iron concentration. This band is used to separate high-iron, schist-hosted emeralds from hydrothermal, low-iron emeralds (e.g., Colombia and Afghanistan).

Various inclusions were seen in the emeralds (figure 3). Very fine fluid inclusions had a blocky outline, sometimes elongated as tubes, with a single bubble inside. In many cases, they were surrounded by a frosty rim that was large enough to obscure the fluid inclusion. No color zoning was observed, but some of the cleaner stones showed wavy to straight graining.

Two types of crystal inclusions were observed, the most common being dark mica platelets and the other consisting

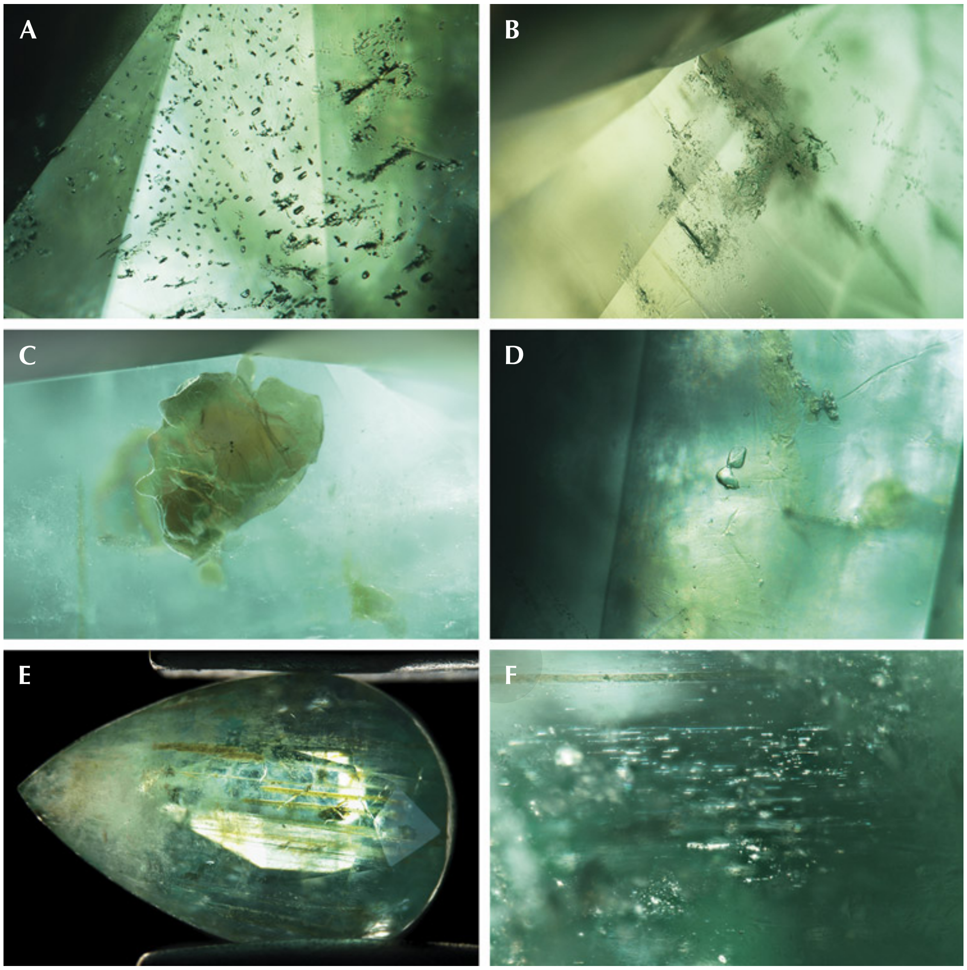

Figure 3. A: A field of blocky two-phase fluid inclusions. B: Elongated two-phase fluid inclusions with large frosty rims. C: An irregularly shaped platy mica crystal. D: Two small, transparent, and colorless feldspar crystals. E: Large tubes filled with a foreign orangy material. F: A cluster of short parallel needles. Photomicrographs by Suwasan Wongchacree; fields of view 1.07 mm (A), 1.80 mm (B, C, and F), 1.20 mm (D), and 10.8 mm (E).

of small transparent colorless crystals. With the use of confocal Raman spectroscopy, some of these transparent crystals were identified as feldspar and others as fluorite. Several stones also showed clusters of short needles mixed with smaller reflective particles, sometimes forming fields of "dusty" particles. A handful of stones had large, wide tubes stained with orangy brown iron mineralization.

Overall, this inclusion scene shares many similarities with samples from other high-iron emerald sources such as Kafubu and Itabira (S. Saeseaw et al., "Geographic origin determination of emerald," Winter 2019 *G&G*, pp. 614–646).

The trace element composition of Curlew emeralds (table 1) allows for separation from other high-iron emerald sources, although multiple elements should be taken into

TABLE 1. Trace element analysis (in ppmw) of 40 emerald samples from Western Australia, measured using LA-ICP-MS (three spots per stone).

	Li	Na	Mg	Sc	V	Cr	Fe	Rb	Cs
Range	260–603	2240–9990	891–7710	21–325	34–444	219–2750	916–4700	13–133	228–2270
Average	377	4093	2345	89	156	1367	1903	38	718
Standard deviation	73	1446	1205	69	85	549	780	22	385
Detection limit (ppmw)	0.05	0.9	0.02	0.09	0.03	0.5	2	0.02	0.01

Figure 4. Two strands of large Japanese akoya bead cultured pearls. The pearls range from 11.0 to 11.6 mm in the top strand and from 11.0 to 12.2 mm in the bottom strand. Photo by Artitaya Homkrajae.

account to clearly separate the Australian emeralds from those found in Russia and Nigeria.

Emeralds from this renewed activity at the Curlew mine in Australia only started to enter the global emerald trade in late 2023. Their appearance and characteristics are in line with other high-iron, schist-hosted emeralds such as those from Zambia, Brazil, and Russia. Inclusions offer limited clues for origin determination, which relies heavily on trace element analysis and correct interpretation of these results.

Wim Vertriest, Suwasan Wongchacree, and Polthep Sakpanich
GIA, Bangkok

Remarkably large akoya bead cultured pearls. Saltwater bead cultured pearls dominating the global pearl market are produced by mollusk species in the *Pinctada* genus, including *P. maxima* (South Sea), *P. margaritifera* (Tahitian), and *P. fucata matensii* (akoya). The size and color of these pearls depend mainly on the mollusk species. The majority of white saltwater bead cultured pearls are South Sea and akoya pearls. South Sea pearls are notable for their large sizes, ranging from 8 to 20 mm, and soft satiny luster. Akoya pearls are well known for their round shape, high degree of luster, and attractive rosé (pink) overtone (very often as a result of processing). Akoya pearls are generally smaller, averaging between 6 and 8 mm in diameter, with those above 10 mm considered rare.

At the 2024 AGTA GemFair in Tucson in February, the author spotted unusually large round akoya pearls that were comparable in size to South Sea bead cultured pearls. These were on display at the booth of Yen's Jewelry & Accessories Inc. (San Francisco). Eric Yen noted that the two strands in figure 4 consisted of the maximum available sizes of Japanese akoya bead cultured pearls. Those in the top strand ranged from 11.0 to 11.6 mm, and those in the bottom strand were

Figure 5. Left: The three-armed claw game (one play for 100 yen). Right: The pearl necklace prize, complete with a jewelry box. Photos by Mari Sasaki (left) and Shunsuke Nagai (right).

between 11.0 and 12.2 mm. Although the bead sizes were not specified, the cultivation process was presumably challenging and required extra caution due to the insertion of a large bead nucleus and possibly the need to nourish the mollusks for several years. Yen explained that these sizes for akoya pearls were extraordinary and multiple harvests were involved to create matching strands. Many mollusks die during the culturing process, which limits production and thus increases rarity and value. In addition to their remarkable sizes, the pearls appeared to have a rounded shape, a spotless surface, high luster, and an appealing rosé overtone.

Artitaya Homkrajae
GIA, Carlsbad

Akoya cultured pearl prize in an arcade-style claw game. Japan began producing pearls in the early 1900s with the successful cultivation of akoya pearls, which are deeply intertwined with the nation's customs. Once used in engagement rings in Japan, akoya pearls remain a jewelry staple for weddings, funerals, and other important occasions. Combining entertainment and product promotion, akoya pearl jewelry began showing up as a prize in Japanese arcades in 2019.

Author MS recently had the opportunity to play a coin-operated "claw" game (figure 5, left) for 100 yen (approximately US$0.65). The prizes offered included earrings, one-size-fits-all unclosed rings, and pendants, all containing akoya pearls. Gold or silver stickers on top of each box indicated the jewelry metal color. After 14 attempts, the author captured the prize shown in figure 5 (right): a pearl set in a 40 cm white metal necklace weighing 2.20 g, contained in a blue jewelry box with a silver sticker but no metal information. According to metal testing by energy-dispersive X-ray fluorescence (EDXRF) spectroscopy, the metal was composed mainly of copper, zinc, and nickel, suggesting an alloy of these metals.

The 8.20 × 8.01 × 7.92 mm pearl had a white bodycolor with pink overtone and was fully drilled with an approximately 1 mm drill hole. The bead was observed through the drill hole. A bumpy surface near the drill hole (figure 6, left) resulted in the pearl's semi-baroque shape. Nacre and terrace structures were observed on the surface (figure 6, right). The pearl's saltwater chemistry was confirmed by EDXRF. Its luster was excellent, and the surface was clean. The pearl fluoresced weak bluish yellow under short-wave UV and moderate bluish yellow under long-wave UV. The fluorescence feature indicates that the pearl had been subjected to a routine set of traditional processes for improving the appearance of cultured pearls (R. Shor, "From single source to global free market: the transformation of the cultured pearl industry," Fall 2007 *G&G*, pp. 200–226). The nacre thickness was measured by optical coherent tomography (OCT),

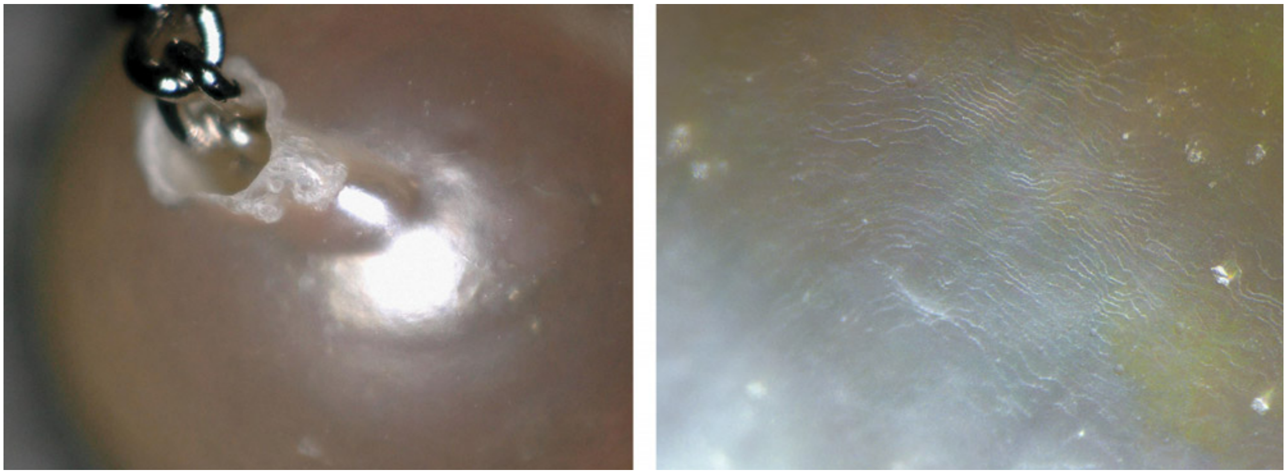

Figure 6. Left: The bumpy surface around the drill hole. Right: Magnification of the pearl surface showing the nacre's terrace structure. Photomicrographs by Mari Sasaki.

a nondestructive technique for cross-sectional imaging of various materials, including pearl and jade (J. Liu et al., "Pearl thickness measurements from optical coherence tomography images," *Applied Mechanics and Materials*, Vol. 421, 2013, pp. 415–420; S. Chang et al., "Detection and analysis of jade material using optical coherence tomography," *Photonics North 2010*, Vol. 7750, 2010, SPIE). The center of the pearl was round with a homogeneous nacre thickness of 0.35 mm ± 0.01 mm (figure 7, left). Toward the drill hole, the thickness was uneven, with some bumpy areas in the thinnest part measuring ~0.23 mm (figure 7, right). Although the quality was very good, the shape was not round and the size was less than 8 mm, which is probably why this pearl became a prize in the claw game.

In addition to arcade games, toy capsule vending machines in commercial locations throughout Japan offer jewelry prizes such as earrings, rings, and pendants using akoya pearls, rough and faceted colored stones, and even diamonds. These machines charge anywhere from 500 to 1,000 yen (approximately US$3.25–$6.50) per try. While claw games allow players to attempt to win the prize of their choice, often unsuccessfully, toy capsule machines dispense a prize every time but by luck of the draw. According to Japanese regulations, the value limit of prizes in crane games is about one thousand yen, so expensive jewelry is not available.

This may be an interesting new outlet for akoya pearls. Those who might not enter a jewelry store can still win a piece of pearl jewelry for themselves, or as small gifts for family and friends.

Mari Sasaki, Kazuko Saruwatari, Shoko Odake, and Tsutomu Takada
GIA, Tokyo

Blister pearl vs. shell blister from *Pteria sterna*. The saltwater mollusk *Pteria sterna*, also known as the rainbow-lipped pearl oyster, is widely distributed in the eastern Pacific, from Baja California to Peru. These mollusks can grow up to 14 cm, producing natural pearls ranging from 3 to 6 mm and rarely up to 11 mm (*CIBJO Pearl Guide*, 2020).

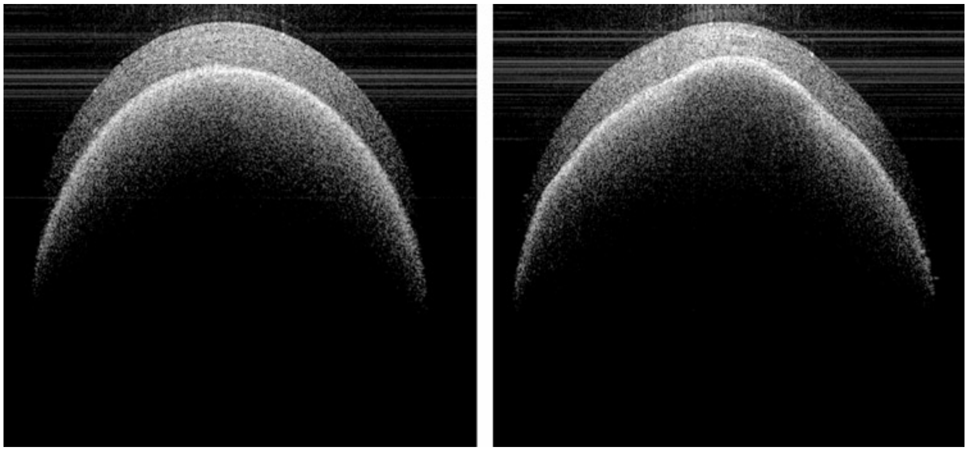

Figure 7. OCT images of the pearl. Left: The middle of the pearl, where the nacre thickness measured ~0.35 mm. Right: The bumpy area, where the nacre thickness measured ~0.23 mm. Images by Kazuko Saruwatari.

Figure 8. These three Pteria sterna *shells each have a visible protuberance, measuring approximately 20.22 × 13.78 × 13.55 mm, 23.49 × 19.06 × 15.62 mm, and 24.88 × 17.03 × 12.23 mm, respectively. Photo by Gaurav Bera.*

Externally, their shells are more concave than those of *Pinctada*-species mollusks, and the internal nacre exhibits vibrant multicolored hues with a metallic sheen. This characteristic is reflected in the wide range of colored pearls they produce.

GIA's Mumbai laboratory recently received a variety of shells for scientific examination. The submission included three shells from *Pteria sterna*, exhibiting nacre colors ranging from brown to gray, with vivid overtones of violet and blue and a strong orient with variations in saturation and tone. The shells weighed 63, 83, and 174 g; each had a prominent protuberance attached to its inner wall, measuring approximately 20.22 × 13.78 × 13.55 mm, 23.49 × 19.06 × 15.62 mm, and 24.88 × 17.03 × 12.23 mm, respectively (figure 8).

Upon examination, dried organic remnants from the aquatic habitat and various parasite intrusion boreholes of differing thickness were observed on all three. Shell 2 in particular had a noticeable cavity in the center of its exterior, which extended into the interior area of the protuberance. A distinct feature observed in all three samples was an irregular, patchy nacreous yellowish brown area, indicative of an adductor muscle scar (figure 9). Viewed under high magnification, the nacreous area revealed spiral patterns of aragonite platelets on the surface (figure 10), similar to those observed in most nacreous pearls from *Pteria*-species mollusks (L. Kiefert et al., "Cultured pearls from the Gulf of California, Mexico," Spring 2004 *G&G*, pp. 26–39).

Energy-dispersive X-ray fluorescence (EDXRF) spectrometry of samples 1 and 3 showed manganese levels of 26 and 110 ppm, and higher strontium levels of 1185 and 1915 ppm, respectively, indicative of their saltwater origin. Due to instrument limitations and the position of sample 2, it was not possible to collect EDXRF data from it. All three samples also exhibited a strong reddish reaction under long-wave ultraviolet light (figure 9) and a weak yellowish reaction under short-wave ultraviolet light. The reddish reaction is linked to a type of porphyrin pigment found in pearls originating from the *Pteria* species (Winter 2014 Lab Notes, pp. 295–296).

Ultraviolet/visible reflectance spectra were collected on multiple spots on the blisters as well as their shells. Absorption bands at identical positions but with different relative intensities were observed at around 405 and 495 nm, indicating a natural color characteristic of the *Pteria* mollusk. Photoluminescence analysis of the pearls revealed the triple bands at 620, 650, and 680 nm, corresponding to their natural coloration (S. Karampelas, "Spectral characteristics of natural-color saltwater cultured pearls from *Pinctada maxima*," Fall 2012 *G&G*, pp. 193–197).

Real-time X-ray microradiography (RTX) imaging of the samples revealed large voids of varying size and opacity, containing organic-rich material of lower opacity with a spotty and granular appearance. However, the images were not clear due to overlapping dark parasitic network structures beneath the growth within the host shells. All three protuberances within the shells displayed a pronounced boundary around the bulge, making them stand out prominently from their host shell. However, the irregularly shaped protuberance observed in shell 1 stood out due to its well-defined outline at the attachment point, forming a clear separation from the shell beneath it. In contrast, the protuberances from shells 2 and 3 appeared to have grown more together with the shell at their bases, lacking clearly

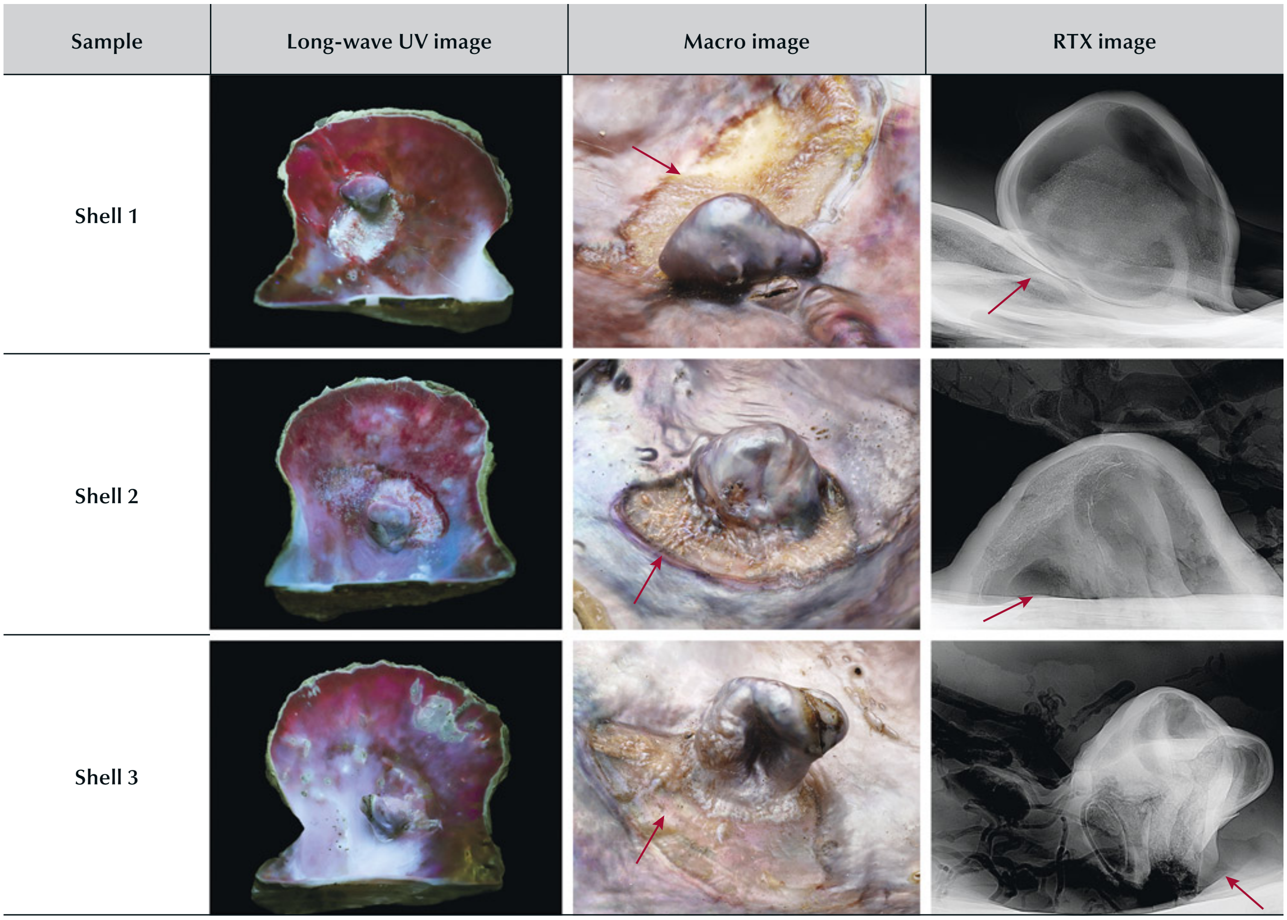

Figure 9. Long-wave UV images displaying a strong red fluorescence typical to that observed in the Pteria *species (left). Macro images showing protuberances and their attachment to the adductor tissue scar beneath (marked with arrows) (middle). RTX images revealing dark organic-rich voids, as well as parasite intrusion and nacre growth at the base (marked with arrows) (right). Photos by Gaurav Bera.*

defined outlines at the attachment points. These features are consistent with RTX observations; sample 1 showed a large organic-rich area followed by a more complete nacre growth around the base, while samples 2 and 3 showed a merging of the bases with the shell growth. Based on the characteristics shown in their base attachment, outline shapes, dome height, and internal growth features, it can be concluded that sample 1 is likely a blister pearl, while samples 2 and 3 lean more toward shell blisters.

Shell blisters result from foreign objects trapped in the space between the mantle tissue and shell, which is subsequently overgrown by layers of calcium carbonate, whereas blister pearls are whole pearls that have perforated from the mantle tissue and attached themselves to the shell (E. Strack, *Pearls*, 2006, Ruhle-Diebener-Verlag GmbH, Stuttgart, pp. 125–127). Previous studies have found that natural shell blisters show some similarities to natural blister pearls in that both have nacreous concre-

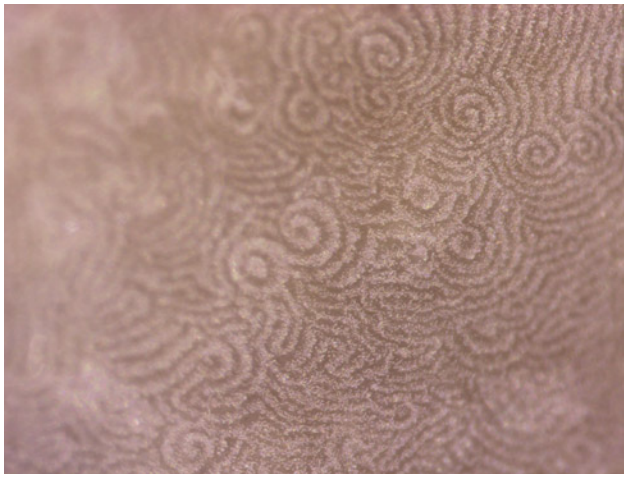

Figure 10. Spiral patterns formed by the platy layers of aragonite (nacre) observed on the surface. Photomicrograph by Lubna Sahani; field of view 1.44 mm.

Figure 11. Haeri Jang's design sketch for the "Blossom" necklace, featuring white gold, pink and colorless diamonds, lavender jade, and akoya pearls.

tions protruding from the inner shell wall ("Natural shell blisters and blister pearls: What's the difference?" *GIA Research News*, August 26, 2019). Differentiating between natural blister pearls and shell blisters remains complex and challenging, relying heavily on external examination and the experience of the gemologist, along with references from observations and research studies. This ongoing learning curve means that even experienced gemologists may reach different conclusions in such cases. GIA is privileged to study such intriguing shell samples, and hopefully these observations will promote a better understanding of natural blister pearls and shell blisters.

Gauri Sarvankar, Lubna Sahani, Roxane Bhot Jain, and Abeer Al-Alawi
GIA, Mumbai

JEWELRY DESIGN

GIA student design showcase. One of GIA's "student choice" awards was recently presented to Haeri Jang, a graduate of the Jewelry Design program at the New York campus. Figure 11 shows Jang's "Blossom" necklace design, which combines white gold, pink and colorless diamonds, lavender jade cabochons, and akoya pearls. Noted Jang, "The inspiration of this piece comes from the ethereal beauty of cherry blossoms. I hope to capture the subtle charm and the timeless elegance of these delicate blooms. I have drawn from my imagination and from both nature and tradition to create this symbol of beauty and purity. I have attempted to modernize the elements of traditional Korean accessories and blend them with a contemporary aesthetic."

SYNTHETICS AND SIMULANTS

A visit to Clarity Diamond's CVD facility. Laboratory-grown diamond sales have surged in the global gem and jewelry market over the past decade. With increased consumer demand, many in the trade are interested in learning more about these products and their supply chain. Firsthand experience, such as visiting a laboratory-grown diamond factory, helps ensure the delivery of reliable information to industry professionals and consumers.

Figure 12. Clarity Diamond opened its CVD facility in Austin to a large group of 2024 AGS Conclave attendees. Scientists led the visitors through the CVD growth process and answered questions from the audience. Courtesy of Clarity Diamond.

Recently, the authors had the opportunity to visit Clarity Diamond's facility in Austin, Texas. We first joined a group tour of around 120 attendees from the 2024 American Gemological Society Conclave (figure 12) and then returned the next day for a more in-depth visit. On both occasions, the Clarity Diamond team openly shared their knowledge of chemical vapor deposition (CVD) diamond growth techniques and products, providing visitors with a rewarding learning experience.

For the majority of the group, including the authors, this was their first visit to a diamond growth facility and the first opportunity to see diamonds growing in a reactor. Attendees participated in engaging demonstrations exhibiting the unique physical properties of polycrystalline CVD-grown diamond. This type of diamond is generally produced as a thin plate composed of thousands of microscopic diamonds and has many applications in other industries such as engineering and electronics. For example, one demonstration showed that polycrystalline diamond could easily cut through ice due to its high thermal conductivity (five times higher than copper), efficiently melting through it (figure 13). Many visitors commented that they wished they had this learning opportunity earlier to help them better understand CVD-grown diamonds or even diamonds in general.

Clarity Diamond's facility hosts a number of reactors as well as a planning and cutting area for research purposes (figure 14). A diamond seed (also referred to as a substrate), a predetermined gas mixture, and extremely hot plasma are the three necessary components to grow CVD diamonds. These diamonds can be produced with interrupted or uninterrupted growth (figure 15). The former requires the grower to remove the crystal from the reactor to polish off unwanted growth and then return it to the reactor. This procedure can be repeated many times, depending on the needs of the grower. In comparison, uninterrupted growth keeps the substrates in the reactor from beginning to end. At Clarity Diamond, the crystals are produced by one un-

Figure 13. Mechanical engineer and product manager A.J. Brown demonstrated diamond's outstanding thermal conductivity for the visitors, who used polycrystalline CVD-grown diamond plates produced in the facility to cut through ice cubes with ease. Courtesy of Clarity Diamond.

interrupted growth cycle. According to founder and CEO Bob Basnett, one of the main challenges in uninterrupted growth is controlling the temperature for an extended time, up to a thousand hours, which allows the crystal to grow continuously to the thickness needed.

These laboratory-grown diamonds are cut and polished by Clarity's partner, HRA Group, at their cutting factory in Ho Chi Minh City, Vietnam. Planning is done by computer-aided tools, and plans are executed following the same cutting and polishing procedures applied to natural

Figure 14. A CVD-grown diamond factory such as Clarity's facility in Austin often has rows of reactors lined up (left). The reactors are carefully monitored throughout the growth period, as demonstrated by process engineer Dr. Amanda Charris (right). Courtesy of Clarity Diamond.

Figure 15. Top: CVD-grown diamond manufacturers grow diamond crystals using seeds (or substrates), a predetermined gas mixture, and plasma of extremely high temperature. Photo courtesy of Clarity Diamond. Bottom: Both interrupted and uninterrupted growth are applied in the industry, and each has advantages and unique challenges. Clarity Diamond uses the uninterrupted method, resulting in CVD-grown diamonds without growth lines, as displayed in this illustration.

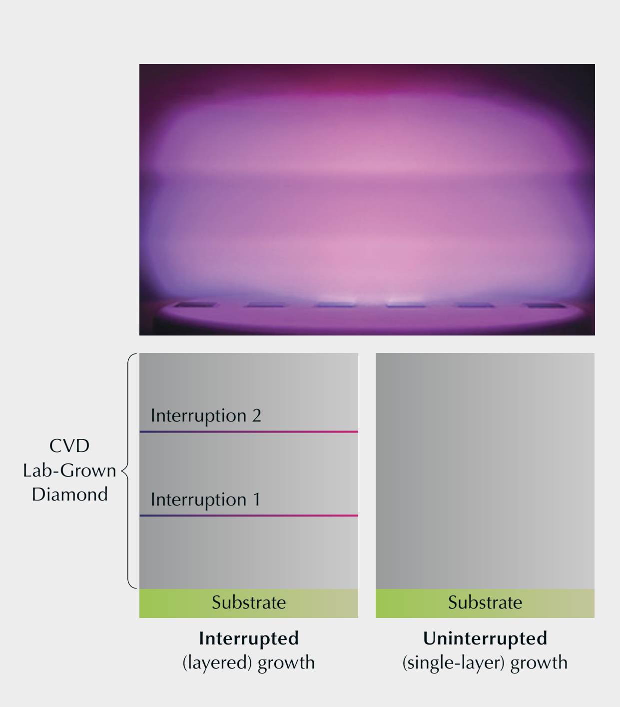

diamonds (figure 16). HRA Group also distributes the finished products to retailers in North America, Australia, and Europe. The brand currently focuses on producing CVD-grown diamonds of high color grade (D–F) and clarity (VS_2 and above).

All visitors, many of whom are jewelry retailers throughout the country, had the chance to view finished jewelry mounted with CVD-grown diamonds manufactured in the facility (figure 17). This gave the retailers the opportunity to understand the product and the process behind the gem, so they can deliver accurate information to consumers. Clarity Diamond is committed to providing transparency about its growth process and business practices to retailers.

Retailer and consumer education remain at the core of our industry and GIA's mission. Education plays an even bigger role when relatively new products are brought to the market. As GIA researchers and educators diligently keep

Figure 16. Planning CVD-grown rough diamond for cutting is done by computer-aided tools, which usually propose options for the cutters—in this case, the two round brilliants to be produced from one rough (left). Then cutters follow processes similar to those used for cutting and polishing natural diamonds (right, 3.16–5.44 ct). Courtesy of Clarity Diamond and HRA Group.

Figure 17. Clarity Diamond hosted a counter inside the facility to show some of its finished jewelry product lines. Courtesy of Clarity Diamond.

up with new developments, we also learn from industry practitioners through opportunities such as this visit to Clarity Diamond's CVD facility.

Tao Hsu and Lisa Kennedy
GIA, Carlsbad and New York

Unusually large flux-grown synthetic sapphire. IIGJ-Research & Laboratories Centre (formerly Gem Testing Laboratory) in Jaipur, India, recently received for identification a translucent blue rough stone weighing 64.70 ct. The specimen appeared transparent in transmitted light and displayed a typical bipyramidal (barrel-shaped) crystal habit along with distinct stepped striations across the surface (i.e., perpendicular to the longer *c*-axis, as shown in figure 18, left). In addition, some areas displayed a rhomb-shaped step pattern, and one side of the bipyramidal crystal had a large rhombohedral face (figure 18, right). This combination of crystal habit and surface features suggested corundum, which was confirmed by Raman spectroscopy.

Under magnification, the specimen displayed white and opaque flux residues in the form of wispy veils or flux fingerprints, along with flux-filled cavities (figure 19). No other inclusions associated with natural or synthetic

Figure 18. This unusually large 64.70 ct rough specimen displaying a bipyramidal crystal habit and stepped striations was identified as a flux-grown synthetic sapphire. Note the large rhombohedral face in the image on right. Photos by Gagan Choudhary.

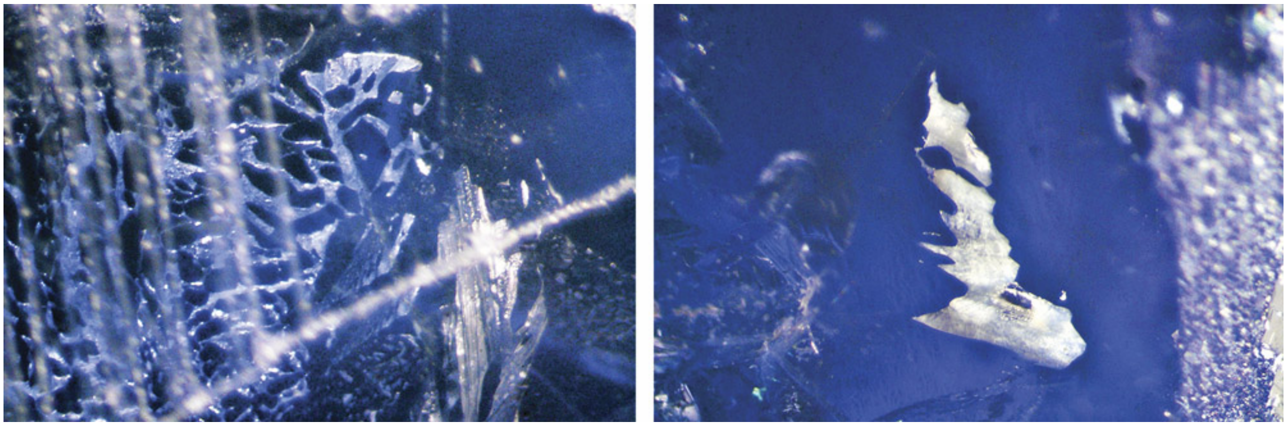

Figure 19. The flux-grown sapphire crystal contained white and opaque flux inclusions in the form of fingerprints (left) and flux-filled cavities (right). Photomicrographs by Gagan Choudhary; field of view 5.08 mm.

corundum were observed. However, the specimen exhibited strong color zoning when immersed in methylene iodide; blue color was mainly concentrated toward the center of the stone, while the rim of the crystal appeared colorless (figure 20). The presence of flux (in the form of fingerprints/cavities) and the absence of any natural inclusions pointed to a synthetic sapphire grown by the flux-fusion process. Under short-wave UV, the specimen displayed strong chalky yellowish green fluorescence while remaining inert under long-wave; such a fluorescence reaction is not observed in natural (heated or unheated) sapphire. Closer examination in the DiamondView revealed stronger yellowish green fluorescence from flux inclusions compared to the stone's body, although zonal greenish fluorescence was also visible. The exact cause of this yellowish green fluorescence remains unknown.

Figure 20. Viewed in immersion, the flux-grown sapphire crystal exhibited strong color zoning, with a deep blue center and a rim that appeared colorless. Photo by Gagan Choudhary.

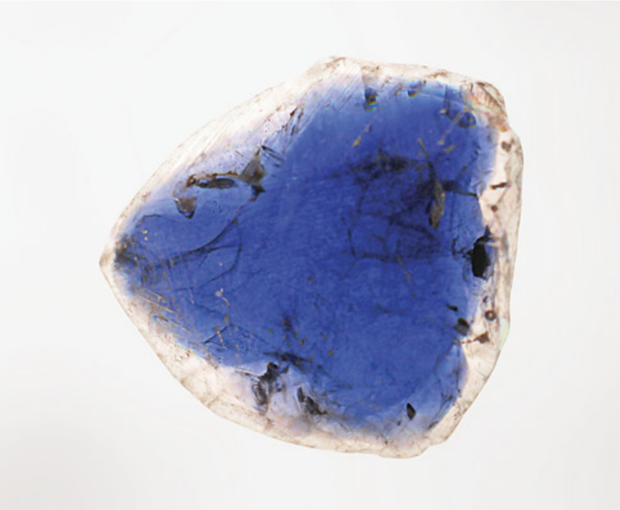

Consistent with an earlier report (Winter 2020 Lab Notes, pp. 524–525), this synthetic sapphire also displayed peaks at ~388 and 450 nm, along with a broad band at ~475–800 nm and an absorption maximum at ~615 nm in its ultraviolet/visible/near-infrared spectrum; these features are associated with Fe^{3+} and Fe^{2+}-Ti^{4+}. Semiquantitative energy-dispersive X-ray fluorescence analysis revealed the presence of molybdenum, tantalum, platinum, and silver, while vanadium and gallium were not detected; this chemistry further indicated a flux-grown synthetic.

This was the first time we had encountered such a large flux-grown synthetic sapphire, though the market availability of this size is unknown. Through careful microscopic observation, along with fluorescence reaction and chemistry, a laboratory gemologist should be able to correctly identify this type of flux-grown synthetic sapphire. But these sapphires, especially in their rough form, may pose a challenge for gem dealers who are generally equipped with a 10× loupe or only basic gemological tools.

Gagan Choudhary (gagan.choudhary@iigjrlc.org)
IIGJ-Research & Laboratories Centre, Jaipur, India

AUCTION REPORTS

Spring 2024 auction highlights. Yellow diamonds brought a ray of sunshine to Geneva for the spring auction season, which was full of excitement in mid-May. The Allnatt diamond, a 101.29 ct Fancy Vivid yellow brilliant set in a brooch designed by Cartier in 1952, was pulled from Sotheby's Magnificent Jewels sale just before it began. Another yellow diamond, the 202.18 ct "Yellow Rose" (figure 21), was the star of Christie's Magnificent Jewels auction the following day. The GIA-graded Fancy Intense yellow

Figure 21. The 202.28 ct "Yellow Rose" diamond sold in Geneva for \$6.7 million. Courtesy of Christie's Images Ltd. 2024.

Figure 22. The "Argyle Phoenix," a 1.56 ct Fancy red diamond, fetched nearly three times its presale estimate. Courtesy of Phillips.

pear modified brilliant with SI_1 clarity sold for \$6.7 million, the second-highest price ever paid at Christie's for a yellow stone weighing more than 200 ct.

Perhaps the most significant highlight in Geneva was the sale of the "Argyle Phoenix" (figure 22), a 1.56 ct Fancy red diamond offered by Phillips that nearly tripled its presale estimate. Selling for \$4.2 million (\$2.7 million per carat), the GIA-graded brilliant set in an 18K gold ring broke two auction records: highest price and highest per-carat price for a Fancy red diamond. Originating from the Argyle mine in Australia, the "Argyle Phoenix" is the largest known Fancy red round brilliant diamond.

Figure 24. The "Eden Rose," a 10.20 ct Fancy Intense pink diamond, surpassed its presale estimate, selling for \$13.3 million. Courtesy of Christie's Images Ltd. 2024.

The trend of exceeding presale estimates continued later in the month at Christie's Magnificent Jewels in Hong Kong. Cartier's multi-gem Tutti Frutti necklace "India" (figure 23) shattered its \$4.9 million high estimate and fetched \$8.7 million. Adorned with carved rubies, emeralds, sapphires, and round GIA-graded diamonds, as well as sapphire, ruby, and emerald beads, the piece sold after 10 minutes of competitive bidding. Christie's reported that more than half the lots in the auction surpassed their estimates, including a "pigeon's blood" Burmese ruby and diamond ring that garnered \$6.4 million, doubling its \$3.2 million high estimate.

At the close of the season in June, Christie's offered the 10.20 ct "Eden Rose" (figure 24) as their top lot in New York. The Internally Flawless Fancy Intense pink type IIa diamond was publicized not only for its size, but also for its pure pink hue and lack of secondary tones. Set in an 18K rose and white gold ring and surrounded by 12 carats of pear- and marquise-shaped colorless diamonds, the GIA-graded round brilliant exceeded its high estimate of \$12 million, selling for \$13.3 million, or \$1.3 million per carat.

Erica Zaidman
GIA, Carlsbad

Figure 23. The "India" necklace from Cartier's Tutti Frutti collection, featuring carved rubies, emeralds, sapphires, and diamonds, nearly doubled its upper presale estimate, garnering $8.7 million in Hong Kong. Courtesy of Christie's Images Ltd. 2024.

Figure 25. A: The show floor at the 2024 IJT. B and C: Yusuke Katsurada's Montana sapphire seminar and a presentation at the GIA booth. Photos by Kazuko Saruwatari (A) and Tomoko Narui (B and C).

CONFERENCE REPORTS

IJT 2024. International Jewelry Tokyo (IJT), held every January at the Tokyo International Exhibition Center, known as Tokyo Big Sight, is Japan's largest jewelry trade show (figure 25). This year, GIA organized a seminar presented by Dr. Yusuke Katsurada titled "The Tales of Montana Sapphire," which focused on colored stone origin and traceability. For the first time, on-site presentations were conducted at the GIA booth, with gemologists from GIA's Tokyo laboratory explaining colored stone treatments to the public.

A variety of items were on display this year. One jewelry maker, Kishun, exhibited AI-designed jewelry (figure 26, left). Spokesperson Hanako Minami noted that this was the company's first such venture. She observed that the AI-generated designs were quite novel but lacked practicality. The company expects AI to learn to produce practical and innovative jewelry designs in the future. Meanwhile, one traditional jeweler presented natural diamond engagement and wedding rings with elaborate designs in metal (figure 26, right). The designs were inspired by floral and other natural elements that have long been familiar in Japanese culture.

Figure 26. Left: These AI-designed rings showcase different themes. From left to right: satellite, cherry blossom, and civil engineering. Right: An engagement ring with a plum blossom design. The side stone is a pink sapphire. Photos by Kazuko Saruwatari; courtesy of Kishun (left) and Manji (right).

Figure 27. Left: Various gemstones with the 180-facet "kikyo" cut, sold loose or set in pendants and rings. Right: A kikyo-cut rutilated quartz. Photos by Kazuko Saruwatari; courtesy of Shimizu Kiseki.

Also on display were gemstones cut with 180 facets, enhancing the brightness of quartz and other materials containing various inclusions (figure 27, left). The facets are based on a dodecahedron structure, with 15 facets on each pentagonal face (figure 27, right). This style is called the "kikyo" cut because of its resemblance to the bellflower (*kikyo* in Japanese). The cut epitomizes the skill of master craftsman Yukio Shimizu, the sole artisan who executes this intricate 180-facet gemstone cut.

Meanwhile, akoya cultured pearls remain popular. Most notable were the akoya pearls from Vietnam, which possessed excellent luster and white color. Vietnamese akoya pearl jewelry was also featured in versatile designs (figure 28, left). Other highlights were South Sea and

Figure 28. Left: Vietnamese akoya pearls are featured in this flexible design for use as a double bracelet or a single choker. Right: Two large South Sea golden pearls and one white pearl larger than 21 mm along with a slightly smaller Tahitian pearl. Photos by Kazuko Saruwatari; courtesy of Spopel (left) and Fiore (right).

Tahitian pearls in sizes larger than 20 mm (figure 28, right).

Next year's IJT will be held January 15–18, 2025, also at Tokyo Big Sight.

Kazuko Saruwatari
GIA, Tokyo

ANNOUNCEMENTS

***G&G* Facebook group surpasses 40,000 members.** In early 2020, *Gems & Gemology* launched a Facebook group dedicated to the world of gemology. Since then, more than 40,000 jewelry professionals, researchers, students, and gem enthusiasts worldwide have joined to share and expand their knowledge. With regular posts from *G&G* contributors and GIA researchers (figure 29), along with posts from group members, followers enjoy a steady stream of content covering gemstone inclusions, treatments, identification, field gemology and mining, and more.

Ready to join? Visit https://www.facebook.com/groups/giagemsgemology to become a member of our growing community.


Sally Eaton Magana

Happy Earth Day! We wanted to celebrate this day and for all that the Earth provides including its fascinating gems and minerals. We're highlighting an interesting Armenian turquoise that was profiled by GIA senior gemologist, **Britni LeCroy**, based in Carlsbad, California. This 84.90 ct stone with natural brown matrix interspersed with the turquoise has a striking resemblance to our Earth. https://www.gia.edu/.../fall-2023-microworld-turquoise...

Figure 29. The Gems & Gemology *Facebook group is a growing community of more than 40,000 gem and jewelry enthusiasts worldwide, featuring posts from* G&G *contributors, GIA researchers, and members of the group.*

ERRATUM

In the Spring 2024 feature article "Nanoscale techniques for characterizing gemstone coatings" by Tsung-Jen Wu et al. (pp. 42–54), carbon and oxygen were inadvertently switched in the legends for figure 3 (left and right). The correct legends are shown below in figure 30. We regret the error.

Figure 30. Corrected legends are shown for the Auger electron spectroscopy plots in figure 3 of Wu et al., "Nanoscale techniques for characterizing gemstone coatings: A case study on synthetic moissanite," from the Spring 2024 issue.